THE JOURNAL OF PHYSICAL CHEMISTRY LETTERS
A JOURNAL OF THE AMERICAN CHEMICAL SOCIETY

pubs.acs.org/JPCL
Letter

Photoelectron Velocity Map Imaging Spectroscopy of the Beryllium Trimer and Tetramer

Noah B. Jaffe, John F. Stanton, and Michael C. Heaven*

Cite This: J. Phys. Chem. Lett. 2023, 14, 8339−8344

ABSTRACT: Computational studies of small beryllium clusters (Be_N) predict dramatic, nonmonotonic changes in the bonding mechanisms and per-atom cohesion energies with increasing N. To date, experimental tests of these quantum chemistry models are lacking for all but the Be_2 molecule. In the present study, we report spectroscopic data for Be_3 and Be_4 obtained via anion photodetachment spectroscopy. The trimer is predicted to have D_{3h} symmetric equilibrium structures for both the neutral molecule and the anion. Photodetachment spectra reveal transitions that originate from the X^2A_2'' ground state and the $1^2A_1'$ electronically excited state. The state symmetries were assigned on the basis of anisotropic photoelectron angular distributions. The neutral and anionic forms of Be_4 are predicted to be tetrahedral. Franck−Condon diagonal photodetachment was observed with a photoelectron angular distribution consistent with the expected $Be_4^-X^2A_1 \rightarrow Be_4X^1A_1$ transition. The electron affinities of Be_3 and Be_4 were determined to be 11363 ± 60 and 13052 ± 50 cm^{-1}, respectively.

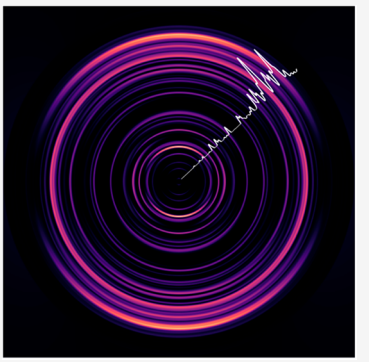

Small beryllium clusters have been the focus of many theoretical studies, with a particular focus on clusters that contain between two and six atoms.[1−23] The bonding in this series is predicted to exhibit dramatic changes as the size of the cluster increases. Be_2 and Be_3 are found to be unbound at the Hartree−Fock self-consistent field (SCF) level of theory.[1,24−26] Bound potential energy wells develop when sufficiently high-level treatments of electron correlation are applied.[1] Be_4 is the first member of the series to be bound at the SCF level. Experimental measurements[20,21,27] show that Be_2, with a formal bond order of 0, is bound with D_e = 934.9 cm^{-1}. This value is appreciably greater than would be expected for a van der Waals interaction between two light closed-shell atoms (e.g., the binding energy for Ne_2 is 29 cm^{-1} [28]). The equilibrium bond length for Be_2 of 2.444 Å is also indicative of a stronger than van der Waals interaction. High-level electronic structure calculations predict that the energy needed to remove an atom from the cluster ($Be_N \rightarrow Be_{N-1} + Be$) has a nonmonotonic dependence on N. For example, Ascik et al.[8] reported atom removal energies of 945, 8470, 22 400, and 13 830 cm^{-1} for N = 2, 3, 4, and 5. This trend is exhibited in the results from both *ab inito* models[7,8,29,30] and density functional theory (DFT)[15,31,32] calculations. A Jellium model[16,32−35] that predicts a superatom closed-shell configuration for Be_4 has been invoked to explain the high dissociation energy for Be_4 and the relatively small dissociation energy for Be_5.

Despite considerable interest in the bonding of Be_N clusters, Be_2 is the only member of the series for which spectroscopic data have been reported.[20,21,27,36−38] To date, our attempts to record electronic spectra for the N > 2 clusters using laser excitation techniques have been unsuccessful. However, Thomas et al.[39] were able to obtain spectroscopic data for Mg_N clusters with N = 3−35 using electron photodetachment spectroscopy of size-selected Mg_N^- cluster anions. For each cluster, they measured the electron affinity (EA) and observed an energy gap between the threshold detachment peak and the onset of features arising from electronically excited states of the neutral cluster. They interpreted the energy intervals as being approximate indicators of the HOMO−LUMO gaps in a Koopman's approximation model. Thomas et al.[39] equated the closing of the HOMO−LUMO gap with the emergence of metallic character.[39,40] The feasibility of performing similar measurements for Be_N clusters was apparent as there were mass spectrometric observations of Be_N^- clusters for the range N = 2−6.[41] The smaller anions have also been the targets of several theoretical studies.[19,25,42,43] Notably, Jordan and Simons[25,42] used SCF models to examine the N = 2, 3, and 4 clusters. They found that the addition of correlation corrections was essential for Be_2^-, but they believed that SCF was sufficient to provide useful insights for the N = 3 and 4 clusters. It is worth noting that later studies performed with correlative treatment gave differing results, both qualitatively and quantitatively, especially with respect to the trimer and its anion.

Received: August 3, 2023
Accepted: September 8, 2023
Published: September 12, 2023

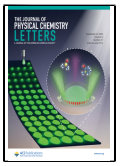

https://doi.org/10.1021/acs.jpclett.3c02169
J. Phys. Chem. Lett. 2023, 14, 8339−8344

More recent calculations have yielded EAs of 4030,[2] 11 125,[43] and 13 530[19] cm^{-1} for N = 2, 3, and 4. Furthermore, the equilibrium structures of the N = 3 and 4 anions and their respective neutrals belong to the same point groups (D_{3h} for N = 3 and T_d for N = 4). Adding an electron to Be_3 is predicted to shorten the bond length, while the bond length of Be_4 is almost unaffected by hosting an extra electron.

Given this history, we used photodetachment spectroscopy of size-selected anions to examine the Be_3 and Be_4 clusters. In these experiments, we applied a slow electron velocity map imaging (SEVI) technique that reveals both the kinetic energies and spatial anisotropies of the photoelectrons.[44] New electronic structure calculations have been carried out using equation of motion electron attachment (EOMEA) coupled cluster formalisms.[45,46] For Be_3^-, these calculations were also used to examine the radiative properties of a long-lived electronically excited state.

The pulsed laser ablation technique used to generate Be_N^- anions provided workable signal levels for Be_3^- and notably more intense signals for Be_4^-. Be_2^- was intermittently present in the ablation products, but the concentration was too low for reliable imaging measurements. Figure 1 shows a survey

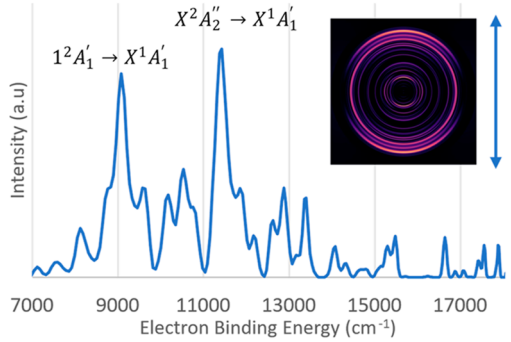

Figure 1. Photoelectron survey spectrum of the Be_3^- anion taken with detachment photon energy of 18 797 cm^{-1} (vertical polarization). The strongest electronic transitions have been labeled with guidance from high-level electronic structure calculations. Inset photo shows the velocity map image produced by MEVELER software

photoelectron spectrum of Be_3^- with an inset velocity map image. Linearly polarized light was used for photodetachment, and the double-headed arrow next to the image shows the orientation of the polarization. The electron binding energy is given by the difference between the energy of the detachment photon and the kinetic energy of the photoelectron. Figure 1 is dominated by two prominent features, separated by approximately 2500 cm^{-1} in energy. Interestingly, with guidance from the high-level theory predictions shown in Table 1, we assign the lower binding energy feature to the $Be_3^-1^2A_1' \rightarrow Be_3X^1A_1'$ transition. This assignment is further supported by the parallel anisotropy present in the velocity map image (anisotropy parameter[44] β = 2), consistent with an $A_1' \rightarrow A_1'$ transition. We have not attempted to assign the weaker features of Figure 1 as they were not reproducible in successive measurements.

An important characteristic of the SEVI technique is that the resolution improves as the photoelectron kinetic energy is reduced.[44] A higher-resolution spectrum of the feature near 9000 cm^{-1} was obtained using 11 236 cm^{-1} (890 nm) detachment photons. The result, shown in Figure 2 along with an inset velocity map image, defined an electron binding

Table 1. Calculated of Transition Energies[a] for Be_3^-

transition	method	basis	energy (cm^{-1})	ΔE_{exp}
$Be_3^-X^2A_2'' \rightarrow Be_3X^1A_1'$	EOMEA-CCSD	aug-cc-pCVTZ	10193	−1170
	EOMEA-CCSD	aug-cc-pCVQZ	10 408	−955
	EOMEA-CCSDT	aug-cc-pCVTZ	11 575	212
	EOMEA-CCSDT	aug-cc-pCVQZ	11 774	411
	MRCI	aug-cc-pV5Z	11 125	−238
	experiment		11 363 ± 60	
$Be_3^-1^2A_1' \rightarrow Be_3X^1A_1'$	EOMEA-CCSD	aug-cc-pCVTZ	7912	−872
	EOMEA-CCSD	aug-cc-pCVQZ	8073	−711
	EOMEA-CCSDT	aug-cc-pCVTZ	8843	59
	EOMEA-CCSDT	aug-cc-pCVQZ	9001	217
	MRCI	aug-cc-pV5Z	8226	−558
	experiment		8784 ± 80	

[a]Comparison of computational and experimental energies. EOM-based methods were computed using the CFOUR package, while MRCI energies are taken from Kalemos.[43] Computational results do not include zero point corrections. ΔE_{exp} lists the difference between the experimental and computational values for the computational results. Zero point corrections for EOMEA-CCSDT using an aug-cc-pCVTZ basis set are +77 cm^{-1} for the $Be_3^-X^2A_2'' \rightarrow Be_3X^1A_1'$ transition and +5 cm^{-1} for the $Be_3^-1^2A_1' \rightarrow Be_3X^1A_1'$ transition.

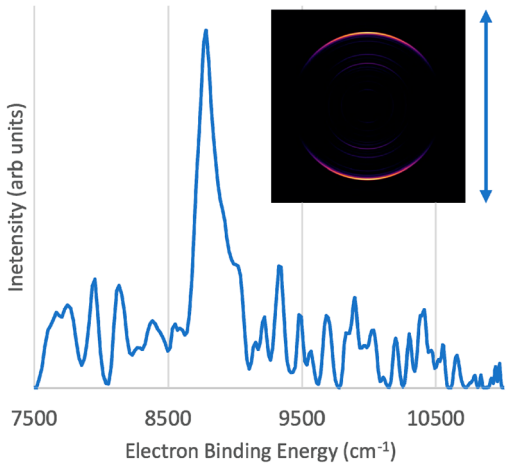

Figure 2. Photoelectron spectrum of Be_3^- taken with a detachment photon energy of 11 236 cm^{-1} (vertical polarization). Inset photo shows the velocity map image produced by MEVELER software

energy of 8784 ± 40 cm^{-1}. Multiple images recorded with the same conditions were analyzed, and the energies of the assignable features were averaged. The quoted uncertainties are 2σ errors that were determined by converting the uncertainties in pixel space from the raw image to the equivalent error in the electron kinetic energy.

The second prominent peak in Figure 1 is assigned to the $Be_3^-X^2A_2'' \rightarrow Be_3X^1A_1'$ origin transition. A higher-resolution spectrum and image for the $Be_3^-X^2A_2'' \rightarrow Be_3X^1A_1'$ transition is presented in Figure 3. This measurement yielded an EA of 11 363 ± 60 cm^{-1}, in good agreement with the present EOMEA-CCSDT calculations (see below) and previously reported MRCI results.[43] The image also shows a reasonable

https://doi.org/10.1021/acs.jpclett.3c02169
J. Phys. Chem. Lett. 2023, 14, 8339−8344

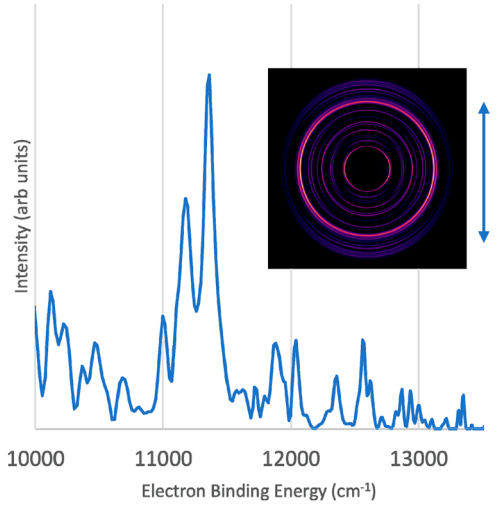

Figure 3. Photoelectron spectrum of Be_3^- taken with a detachment photon energy of 13 605 cm^{-1} (vertical polarization). Inset photo shows the velocity map image produced by MEVELER software

degree of perpendicular anisotropy, with $\beta = -0.5 \pm 0.3$, which is supportive of the predicted symmetries of the electronic states involved in this transition. Interestingly, because smaller intensity peaks energetically just below the EA peak have near parallel anisotropy, the anisotropy of the EA peak in the survey spectrum (Figure 1 inset) appears to show s-wave detachment. This apparent s-wave detachment is an artifact of these different peaks collapsing to almost the same radius under the survey conditions, and the high intensity part of the peak still shows an anisotropy value of $\beta = -0.5 \pm 0.3$.

To gain further insight into the experimental data, *ab inito* computations were carried out using the CFOUR package.[47] Dunning correlation consistent basis sets[48] were used along with several different coupled-cluster treatments.[45,46,49,50] Electronic energy predictions are presented in Table 1. Geometry optimizations are presented in Table 2, and the results from vibrational harmonic frequency calculations are included in the Supporting Information (Table S1).

Table 2. Bond Lengths of Be_3 and Be_3^-

		bond length (Å)		
method	basis	$Be_3X^1A_1'$	$Be_3^-X^2A_2''$	$Be_3^-1^2A_1'$
MRCI	aug-cc-pV5Z	2.203	2.106	2.177
CCSD	aug-cc-pCVTZ	2.218	2.129	2.195
CCSD	aug-cc-pCVQZ	2.201	2.116	2.179
CCSDT	aug-cc-pCVDZ	2.247	2.150	2.216
CCSDT	aug-cc-pCVTZ	2.206	2.114	2.180
CCSDT	aug-cc-pCVQZ	2.191	2.102	2.167

Predictions using the EOMEA-CCSDT method and the aug-cc-pcVTZ basis set were found to provide a better treatment of these transitions than any other method tested when comparing the experimentally determined transition energies to the computational predictions. Interestingly the EOMEA-CCSDT calculations both overestimate the EA of this molecule, with the aug-cc-pcVQZ computation overestimating slightly more than the aug-cc-pcVTZ computation. This may imply that, even with the aug-cc-pcVTZ basis set, the neutral is already almost converged to the CCSDT complete basis limit, while the anion has not reached this limit. Hence, the energy of the anion shifts further down below that of the neutral molecule when the basis set is increased from VTZ to VQZ. More accurate predictions would require a method that accounts for higher order correlation effects like CCSDTQ. As can be seen from the comparison with EOMEA-CCSD, the role of triple excitations is very important to this system, leading to EOMEA-CCSD under-converging the anion states substantially and leading to an EA value approximately 1000 cm^{-1} below the experimental value (not including zero-point energy contributions). It does however appear that EOMEA-CCSD is sufficient to determine the geometry of this molecule, with the bond length being the same within ~0.02 Å as compared to EOMEA-CCSDT and MRCI. The previously published MRCI/aug-cc-pV5Z results[43] also agree well with the EOMEA-CCSDT geometries and come close to the experimental values, differing by about 230 cm^{-1} when considering the EA. It is possible that a core−valence basis set would tip the scales in favor of the MRCI method for this molecule, as computations of Be-containing molecules often require the inclusion of core−core and core−valence correlation to be accurately computed, and this phenomenon has been predicted to be substantial for pure Be clusters like Be_3 as well.

The $Be_3^-1^2A_1' \rightarrow Be_3X^1A_1'$ and $Be_3^-X^2A_2'' \rightarrow Be_3X^1A_1'$ transitions were observed to have comparable intensities (c.f. Figure 1) under jet cooling conditions, where the X^2A_2'' state would be expected to have a greater population than the $1^2A_1'$ state. Hence, the comparable intensities suggest that the threshold photodetachment cross section for the $1^2A_1'Be_3^- \rightarrow Be_3X^1A_1'$ transition is greater than that for $Be_3^-X^2A_2'' \rightarrow Be_3X^1A_1'$. This difference in cross sections is consistent with what may be expected based on the results from computational geometry optimizations.

The relevant bond lengths are shown in Table 2, and the CCSDT (neutral) and EOM-CCSDT (anion) potential energy curves for the symmetric stretch using an aug-cc-pCVTZ basis set are shown in Figure 4. The bond length and shape of the potential curve of the $Be_3^-1^2A_1'$ state is nearly identical to the properties of the $Be_3X^1A_1'$ state, in contrast to the shorter

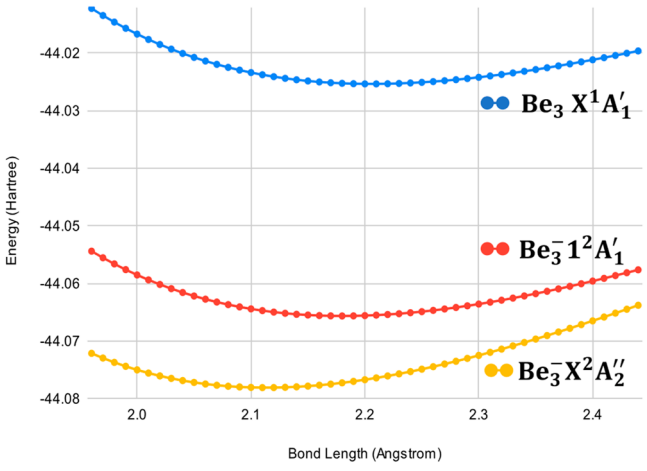

Figure 4. Potential energy curves for the Be_3^- anion and neutral molecule between 1.95 Å and 2.44 Å, computed in 0.01 Å steps along the symmetric stretch. The neutral ground state was computed using CCSDT, and the anion states were computed using EOMEA-CCSDT. All computations were performed in CFOUR using an aug-cc-pCVTZ basis set.

https://doi.org/10.1021/acs.jpclett.3c02169
J. Phys. Chem. Lett. 2023, 14, 8339−8344

bond length and slightly steeper curvature of the $Be_3^-X^2A_2''$ potential energy function. Hence, the near vertical Franck–Condon profile of the $Be_3^-1^2A_1' \rightarrow Be_3X^1A_1'$ transition may partially account for the higher-than-expected intensity for transitions originating from the anion excited state, as compared to the smaller, less vertical Franck–Condon profile of the $Be_3^-X^2A_2'' \rightarrow Be_3X^1A_1'$ transition. Surprisingly, neither the survey spectrum (Figure 1) nor the higher-resolution spectrum (Figure 2) showed an obvious progression in the totally symmetrical stretch, although an observable progression was predicted by a Franck–Condon simulation based on the symmetric stretch potential energy curves (see the Supporting Information). It is possible that the small peaks at energies above the EA transition were produced by excited vibrational levels in the neutral ground state, but they were not repeatable enough in our study to warrant assignment.

Our ability to consistently image the transition originating from the $Be_3^-1^2A_1'$ state suggests that this state has a lifetime of 100 μs or more, based on the time it takes for an anion to reach the position where photodetachment occurs in our apparatus. This is substantially longer than may be expected considering that decay to the anion ground state is (by symmetry) allowed by the electric dipole moment. To determine if this long-lived excited state hypothesis was physically reasonable, the oscillator strength was calculated at the EOMEE-CCSD level with an aug-cc-pCVTZ basis set for the $Be_3^-1^2A_1' \rightarrow Be_3^-X^2A_2''$ transition. The oscillator strength was found to be approximately 7.4×10^{-5}, consistent with an Einstein A coefficient of 330 s^{-1} and a radiative lifetime of 3024 μs when using the experimentally determined energy gap, or an Einstein A coefficient of 2320 s^{-1} and lifetime of 431 μs when using the energy gap from the calculation that provided the oscillator strength. In either case, this lifetime is substantially longer than the ~100 μs flight time in our experiment and longer than the lifetime of any other anion excited state that has a dipole allowed transition to the ground state that we have been able to find in the literature. This long lifetime can be partially explained by looking at the shapes of the $1^2A_1'$ and X^2A_2'' potential energy curves with respect to bond length as seen in Figure 4. The excited $1^2A_1'$ anion state has substantially different curvature at the bottom of the well as compared to the ground X^2A_2'' anion state, which likely leads to a lower vibrational wave function overlap. The inability to relax from the $Be_3^-1^2A_1'$ excited state within the time of our experiment, as well as the strong vibrational wave function overlap with the neutral ground state, leads to the $Be_3^-1^2A_1' \rightarrow Be_3X^1A_1'$ transition showing substantial intensity in all spectra we have taken of this anion.

The photodetachment spectrum and electron velocity map image for Be_4^- are shown in Figure 5. This trace is dominated by a single peak and exhibits a clear preference for the ejection of electrons along the polarization vector of the light used for photodetachment. A higher-resolution trace (included in the Supporting Information, Figure S1) yielded an adiabatic EA of 13 052 ± 50 cm^{-1}. The simplicity of this spectrum was readily anticipated by using previously published computational results for Be_4 and Be_4^-. For example, Diaz et al.[19] examined Be_4 and Be_4^- using MP2 and ROMP2 methods with basis sets of triple and quadruple-ζ quality. They found that adding an electron to Be_4 had a minimal effect on the bond length, causing a contraction of just 0.02 Å. Be_4 has a closed-shell $\tilde{X}^1A_1$ ground state and the unpaired electron of Be_4^- resides in an orbital of A_1 symmetry. The latter is primarily an in-phase

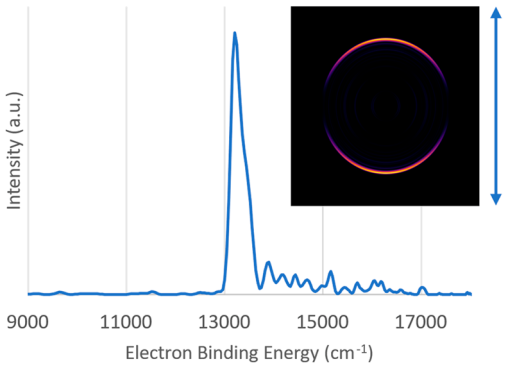

Figure 5. Photoelectron spectrum of Be_4^- taken with a detachment photon energy of 18 182 cm^{-1} (vertical polarization). Inset photo shows the velocity map image produced by MEVELER software.

linear combination of sp hybrids that point toward the center of the tetrahedron.[19] This appears to be a nonbonding orbital and yields an $\tilde{X}^2A_1$ ground state for the anion. Hence, the dominant single peak of the spectrum and the parallel anisotropy of the $Be_4^-\tilde{X}^2A_1 \rightarrow Be_4\tilde{X}^1A_1$ photodetachment image are in qualitative agreement with the computational predictions. The quantitative agreement between the measured and calculated EA values for Be_4 is also acceptable. Diaz et al.[19] obtained the same value for both the vertical and adiabatic EAs of 13 534 cm^{-1}, which is 482 cm^{-1} above the measured value. Our CCSD(T) calculations with the aug-cc-pVTZ basis set gave a vertical EA value of 12 718 cm^{-1}, underestimating the measured value by 334 cm^{-1}. This result and the calculated harmonic vibrational frequencies for Be_4 and Be_4^- are listed in Table S2 of the Supporting Information.

Higher energy photoelectron spectra for Be_3^- and Be_4^- were recorded by using 355 and 395 nm photodetachment, respectively. These wavelengths provided observation windows for states with internal energies of up to 16 800 cm^{-1} (Be_3) and 12 264 cm^{-1} (Be_4). These energies are well above most computational predictions of the triplet excited state energies.[15−17] In the case of Be_3, weak transitions were observed in the energy range approximately 6140 to 10640 cm^{-1} above the ground state zero-point level but without strong enough repeatable features to be reliably assigned. We believe this is due to the predicted Jahn–Teller distortion of the Be_3 geometry in its first excited triplet state (reducing the symmetry to C_{2v}), which lowers the Franck–Condon overlap to these excited states and prevents adequate intensity to assign these features when combined with the already weak signal from Be_3^-. In Be_4, the first excited electronic state has also been predicted to be a triplet state that is subject to Jahn–Teller effects, reducing the symmetry from T_d to either C_{2v} or D_{2d} depending on the computational method of prediction. We observed a reasonable amount of spectral activity in the energy range 7950–10 950 cm^{-1} above the Be_4 origin, in qualitative agreement with expectations of the singlet–triplet gap in the tetramer. However, the spectra were extremely congested, likely due to Jahn–Teller splitting of the triplet.

A number of trends have been delineated in the theoretical studies of small beryllium clusters carried out to date. It has been established that high-level electron correlation treatments are needed for the beryllium dimer and that electron correlation becomes less important as the cluster size increases. The rapid increase of the binding energy in the sequence N = 2–4 has been traced to increasing s–p hybridization and

https://doi.org/10.1021/acs.jpclett.3c02169
J. Phys. Chem. Lett. 2023, 14, 8339−8344

many-body interactions. The present experimental results for Be_3 and Be_4 help to validate the predictive capabilities of the high-level computational models that revealed the above-mentioned trends. This indicates that our developing qualitative understanding of the bonding in Be_N clusters is on the right track.

EXPERIMENTAL METHODS

Photodetachment spectra of the Be_3^- and Be_4^- anions were obtained by using a slow electron velocity map imaging spectrometer. This instrument has been described previously.[51,52] It was recently updated to use an Even-Lavie-type pulsed valve, replacing the previous Jordan-type pulsed valve. Anions were generated by pulsed laser ablation of a pure beryllium rod using the fundamental output of a Nd:YAG laser (1064 nm). The ablation products were entrained in a carrier gas that consisted of approximately 1% nitrogen in argon. The N_2 was included as it appeared to be an effective third body collider to stabilize cluster anion formation. Anions from the ablation source were expansion-cooled, mass selected, and then photodetached using the harmonics of an Nd:YAG laser (532 and 355 nm) or tunable radiation from a pulsed dye laser (395 nm) or an OPO laser (720−890 nm). The lasers were linearly polarized with a vertical orientation for all measurements. Photoelectron images were accumulated using in-house software that only saved individual "shots" with higher levels of signal to lower the background noise contribution to the image. This was necessary as the yields of beryllium anion clusters were low, and the production was intermittent. The raw velocity map images were processed using the MEVELER[53] software package, and energy calibrations were performed using the known transitions of S^- recorded for various photodetachment wavelengths.

ASSOCIATED CONTENT

Supporting Information

The Supporting Information is available free of charge at https://pubs.acs.org/doi/10.1021/acs.jpclett.3c02169.

Calculated vibrational frequencies for Be_3 and Be_3^-, near-threshold photodetachment image and spectrum for Be_4^-, calculated Franck−Condon factors for the $2A_1'-2A_2''$ transition of Be_3^-, calculated values for the electron affinity of Be_4, calculated vibrational frequencies for Be_4 and Be_4^- (PDF)

Transparent Peer Review report available

AUTHOR INFORMATION

Corresponding Author

Michael C. Heaven − *Department of Chemistry, Emory University, Atlanta, Georgia 30322, United States;* orcid.org/0000-0003-4738-2408; Phone: (404) 727-6617; Email: mheaven@emory.edu

Authors

Noah B. Jaffe − *Department of Chemistry, Emory University, Atlanta, Georgia 30322, United States*

John F. Stanton − *Department of Chemistry - Quantum Theory Project, University of Florida, Gainesville, Florida 32611, United States;* orcid.org/0000-0003-2345-9781

Complete contact information is available at: https://pubs.acs.org/10.1021/acs.jpclett.3c02169

Notes

The authors declare no competing financial interest.

ACKNOWLEDGMENTS

The authors acknowledge the support of the U.S. Department of Energy, Office of Basic Energy Sciences under award DE-SC0018163 and the National Science Foundation under grant CHE- 2055579. The authors would additionally like to acknowledge David A. Stewart for their participation in the measurements for Be_4.

REFERENCES

(1) Heaven, M. C.; Merritt, J. M.; Bondybey, V. E. Bonding in beryllium clusters. *Annu. Rev. Phys. Chem.* **2011**, *62*, 375−393.

(2) Kalemos, A. The nature of the chemical bond in Be_2^+, Be_2, Be_2^-, and Be_3. *J. Chem. Phys.* **2016**, *145*, 214302/214301−214302/214313.

(3) Deible, M. J.; Kessler, M.; Gasperich, K. E.; Jordan, K. D. Quantum Monte Carlo calculation of the binding energy of the beryllium dimer. *J. Chem. Phys.* **2015**, *143*, 084116/084111−084116/084115.

(4) Sharma, S.; Yanai, T.; Booth, G. H.; Umrigar, C. J.; Chan, G. K.-L. Spectroscopic accuracy directly from quantum chemistry: Application to ground and excited states of beryllium dimer. *J. Chem. Phys.* **2014**, *140*, 104112/104111−104112/104118.

(5) Mentel, L. M.; Baerends, E. J. Can the counterpoise correction for basis set superposition effect be jstified? *J. Chem. Theo, Comput.* **2014**, *10*, 252−267.

(6) El Khatib, M.; Bendazzoli, G. L.; Evangelisti, S.; Helal, W.; Leininger, T.; Tenti, L.; Angeli, C. Beryllium dimer: a bond bsed on non-dynamical correlation. *J. Phys. Chem. A* **2014**, *118*, 6664−6673.

(7) Sulka, M.; Labanc, D.; Kovac, M.; Pitonak, M.; Cernusak, I.; Neogrady, P. Ab initio study of the stability of beryllium clusters. Accurate calculations for Be_{2-6}. *J. Phys. B At., Mol. Opt. Phys.* **2012**, *45*, 085102.

(8) Ascik, P. N.; Rugango, R.; Simmonett, A. C.; Compaan, K. R.; Schaefer, H. F. The Beryllium pentamer: trailing an uneven sequence of dissociation energies. *ChemPhysChem* **2012**, *13*, 1255−1260.

(9) Le Roy, R. J.; Haugen, C. C.; Tao, J.; Li, H. Long-range damping functions improve the short-range behaviour of 'MLR' potential energy functions. *Mol. Phys.* **2011**, *109* (3), 435−446.

(10) Koput, J. The ground-state potential energy function of a beryllium dimer determined using the single-reference coupled-cluster approach. *Phys. Chem. Chem. Phys.* **2011**, *13* (45), 20311−20317.

(11) Diaz-Torrejon, C. C.; Kaplan, I. G. Many-body forces and stability of the alkaline-earth tetramers. *Chem. Phys.* **2011**, *381*, 67−71.

(12) Schmidt, M. W.; Ivanic, J.; Ruedenberg, K. Electronic structure analysis of the ground-state potential energy curve of Be_2. *J. Phys. Chem. A* **2010**, *114*, 8687−8696.

(13) Vetere, V.; Monari, A.; Scemama, A.; Bendazzoli, G. L.; Evangelisti, S. A theoretical study of linear beryllium chains: Full configuration interaction. *J. Chem. Phys.* **2009**, *130*, 024301−0243019.

(14) Patkowski, K.; Spirko, V.; Szalewicz, K. On the elusive twelfth vibrational state of beryllium dimer. *Science* **2009**, *326*, 1382−138.

(15) Beyer, M. K.; Kaledin, L. A.; Kaledin, A. L.; Heaven, M. C.; Bondybey, V. E. Density functional calculations of beryllium clusters Be_n, n = 2−8. *Chem. Phys.* **2000**, *262*, 15−23.

(16) Srinivas, S.; Jellinek, J. Structural and electronic properties of small beryllium clusters: A theoretical study. *J. Chem. Phys.* **2004**, *121*, 7243−7252.

(17) Cerowski, V.; Rao, B. K.; Khanna, S. N.; Jena, P.; Ishii, S.; Ohno, K.; Kawazoe, Y. Evolution of the electronic structure of Be clusters. *J. Chem. Phys.* **2005**, *123*, 074329/074321−074329/074310.

(18) Junquera-Hernandez, J. M.; Sanchez-Marin, J.; Bendazzoli, G. L.; Evangelisti, S. Full configuration interaction calculation of Be_3. *J. Chem. Phys.* **2004**, *120*, 8405−8411.

(19) Diaz, C. C.; Kaplan, I. G.; Roszak, S. Theoretical study of the electron affinities of the alkaline-earth tetramers possessing T_d symmetry: Be_4 and Mg_4. *J. Mol. Model.* **2005**, *11*, 330−334.
(20) Bondybey, V. E.; English, J. H. Laser vaporization of beryllium: gas phase spectrum and molecular potential of diatomic beryllium. *J. Chem. Phys.* **1984**, *80*, 568−570.
(21) Bondybey, V. E. Electronic structure and bonding of diatomic beryllium. *Chem. Phys. Lett.* **1984**, *109*, 436−441.
(22) Kaplan, I. G. Many-body interactions, symmetry adapted perturbation theory, and chemical bonding in beryllium clusters. *Polym. J. Chem.* **1998**, *72*, 1454−1463.
(23) Kaplan, I. G. Role of electron correlation in nonadditive forces and ab initio model potentials for small metal clusters. *Adv. Quantum Chem.* **1998**, *31*, 137−156.
(24) Klos, J.; Zuchowski, P. S.; Rajchel, L.; Chalasinski, G.; Szczesniak, M. M. Nonadditive interactions in ns^2 and spin-polarized ns metal atom trimers. *J. Chem. Phys.* **2008**, *129*, 134302/134301−134302/134309.
(25) Jordan, K. D.; Simons, J. Electronic structure of small metal clusters. I. Anions of diatomic, triatomic, and tetraatomic beryllium. *J. Chem. Phys.* **1977**, *67*, 4027−4037.
(26) Lee, T. J.; Rendell, A. P.; Taylor, P. R. Theoretical investigations of the structures and binding energies of beryllium and magnesium (Be_n and Mg_n (n = 3−5)) clusters. *J. Chem. Phys.* **1990**, *92*, 489−495.
(27) Merritt, J. M.; Bondybey, V. E.; Heaven, M. C. Beryllium dimer-caught in the act of bnonding. *Science* **2009**, *324*, 1548−1551.
(28) Tang, K. T.; Toennies, J. P. The van der Waals potentials between all of the rare gas atoms from He to Rn. *J. Chem. Phys.* **2003**, *118*, 4976−4983.
(29) Sulka, M.; Pitonak, M.; Cernusak, I.; Urban, M.; Neogrady, P. Ab initio study of many-body decomposition of the interaction energy in small beryllium clusters Be_{3-6}. *Chem. Phys. Lett.* **2013**, *573*, 8−14.
(30) Ascik, P. N.; Wilke, J. J.; Simmonett, A. C.; Yamaguchi, Y.; Schaefer, H. F., III. The Beryllium tetramer: profiling an elusive molecule. *J. Chem. Phys.* **2011**, *134*, 074110/074111−074110/074118.
(31) Bakhsh, S.; Liu, X.; Wang, Y.; He, L.; Ren, X. Beryllium and magnesium metal clusters: new globally stable structures and G_0W_0 Calculations. *J. Phys. Chem. A* **2021**, *125*, 1424−1435.
(32) Abyaz, B.; Mahdavifar, Z.; Schreckenbach, G.; Gao, Y. Prediction of beryllium clusters (Be_n; n = 3−25) from first principles. *Phys. Chem. Chem. Phys.* **2021**, *23*, 19716−19728.
(33) Sun, Y.; Fournier, R. Density functional study of beryllium clusters. *Comp. Lett.* **2005**, *1*, 210−219.
(34) Poater, J.; Sola, M. Open-shell jellium aromaticity in metal clusters. *Chem. Commun.* **2019**, *55*, 5559−5562.
(35) Kolchin, A. M.; Hall, R. W. Electronic properties of small neutral and charged beryllium clusters. *J. Chem. Phys.* **2000**, *113*, 4083−4092.
(36) Antonov, I. O.; Barker, B. J.; Bondybey, V. E.; Heaven, M. C. Spectroscopic characterization of Be_2^+ X $^2\Sigma_u^+$ and the ionization energy of Be_2. *J. Chem. Phys.* **2010**, *133*, 074309/074301−074309/074304.
(37) Merritt, J. M.; Kaledin, A. L.; Bondybey, V. E.; Heaven, M. C. The ionization energy of Be2, and spectroscopic characterization of the $(1)^3\Sigma^+_u$, $(2)^3\Pi_g$, and $(3)^3\Pi_g$ states. *Phys. Chem. Chem. Phys.* **2008**, *10*, 4006−4013.
(38) Kaledin, L. A.; Kaledin, A. L.; Heaven, M. C.; Bondybey, V. E. Electronic structure of Be_2: theoretical and experimental results. *THEOCHEM* **1999**, *461−462*, 177−186.
(39) Thomas, O. C.; Zheng, W. J.; Xu, S. J.; Bowen, K. H. Onset of metallic behavior in magnesium clusters. *Phys. Rev. Lett.* **2002**, *89*, 213403−213401.
(40) Acioli, P. H.; Jellinek, J. Electron Binding Energies of anionic magnesium clusters and the nonmetal-to-metal transition. *Phys. Rev. Lett.* **2002**, *89*, 213402/213401−213402/213404.
(41) Middleton, R.; Klein, J. Production of metastable negative ions in a cesium sputter source: Verification of the existence of N_2^- and CO. *Phys. Rev. A* **1999**, *60*, 3786−3799.
(42) Jordan, K. D.; Simons, J. Comment on the electronic structure of small beryllium and magnesium clusters and their anions. *J. Chem. Phys.* **1980**, *72*, 2889−2890.
(43) Kalemos, A. Be_3^-, an ab initio study. *Chem. Phys. Lett.* **2020**, *739*, 136964.
(44) Neumark, D. M. Slow electron velocity-map imaging of negative ions: applications to spectroscopy and dynamics. *J. Phys. Chem. A* **2008**, *112*, 13287−13301.
(45) Nooijen, M.; Bartlett, R. J. Equation of motion coupled cluster method for electron attachment. *J. Chem. Phys.* **1995**, *102*, 3629−3647.
(46) Stanton, J. F.; Bartlett, R. J. The equation of motion coupled-cluster method. A systematic biorthogonal approach to molecular excitation energies, transition probabilities, and excited state properties. *J. Chem. Phys.* **1993**, *98*, 7029−7039.
(47) Matthews, D. A.; Cheng, L.; Harding, M. E.; Lipparini, F.; Stopkowicz, S.; Jagau, T. C.; Szalay, P. G.; Gauss, J.; Stanton, J. F. Coupled-cluster techniques for computational chemistry: The CFOUR program package. *J. Chem. Phys.* **2020**, *152*, 214108.
(48) Prascher, B. P.; Woon, D. E.; Peterson, K. A.; Dunning, T. H.; Wilson, A. K. Gaussian basis sets for use in correlated molecular calculations. VII. Valence, core-valence, and scalar relativistic basis sets for Li, Be, Na, and Mg. *Theor. Chem. Acc.* **2011**, *128*, 69−82.
(49) Kucharski, S. A.; Włoch, M.; Musiał, M.; Bartlett, R. J. Coupled-cluster theory for excited electronic states: The full equation-of-motion coupled-cluster single, double, and triple excitation method. *J. Chem. Phys.* **2001**, *115*, 8263−8266.
(50) Stanton, J. F. Many-body methods for excited state potential energy surfaces. I. General theory of energy gradients for the equation-of-motion coupled-cluster method. *J. Chem. Phys.* **1993**, *99*, 8840−8847.
(51) Mascaritolo, K. J.; Dermer, A. R.; Green, M. L.; Gardner, A. M.; Heaven, M. C. Photodetachment spectroscopy of the beryllium oxide anion, BeO^-. *J. Chem. Phys.* **2017**, *146*, 054301/054301−054301/054306.
(52) Dermer, A. R.; Green, M. L.; Mascaritolo, K. J.; Heaven, M. C. Photoelectron velocity map imaging spectroscopy of the beryllium sulfide anion, BeS^-. *J. Phys. Chem. A* **2017**, *121*, 5645−5650.
(53) Dick, B. Inverting ion images without Abel inversion: maximum entropy reconstruction of velocity maps. *Phys. Chem. Chem. Phys.* **2014**, *16*, 570−580.

https://doi.org/10.1021/acs.jpclett.3c02169
J. Phys. Chem. Lett. 2023, 14, 8339−8344